ACMEG-T: Soil Thermoplasticity Model

Lyesse Laloui[1] and Bertrand François[2]

Abstract: This paper addresses an advanced and unified thermomechanical constitutive model for soils. Based on experimental evidence showing the nonlinear and irreversible thermomechanical responses of saturated soils, the constitutive equations of the developed model, Advanced Constitutive Model for Environmental Geomechanics-Thermal effect (ACMEG-T), are presented. In the context of elastoplasticity and critical state theory, the model uses the multimechanism plasticity and bounding surface theory. Nonlinear thermoelasticity is joined with two coupled thermoplastic dissipative processes. The yield functions, the dissipative potentials and the plastic multipliers are introduced. Attention is particularly focused on the coupling between both plastic mechanisms, an isotropic and a deviatoric one, which are in agreement with the consistency condition for multiple dissipation. As far as isotropic mechanism is concerned, a unique thermomechanical yield surface reproduces the thermoplasticity observed at low and intermediate overconsolidation ratios, as well as the plasticity under mechanical loading in an framework unifying mechanical and thermal hardenings. Finally, the efficiency of ACMEG-T is proven by validation tests on drained and undrained thermomechanical paths.

DOI: 10.1061/(ASCE)EM.1943-7889.0000011

CE Database subject headings: Plasticity; Constitutive model; Thermal factors; Soils.

Introduction

There are many applications related to the thermomechanical behavior of soils, notably for high-level nuclear waste disposal (Laloui and Modaressi 2002), heat storage (Burger et al. 1985), geothermal structures (Laloui et al. 2003,2006; Brandl 2006), petroleum drilling, injection and production activities, zones around buried high-voltage cables (Mitchell et al. 1982) as well as others related to seasonal and daily cyclical temperature variations, such as road subgrades, furnace foundations, not to mention sample disturbance due to temperature changes during sampling, storage, and testing. Due to the importance of such applications, the thermomechanical behavior of soils is becoming one of the major issues in environmental geomechanics (Vulliet et al. 2002).

This paper deals with the constitutive modeling of the nonisothermal mechanical behavior of soils. It aims to present the outcome of ongoing developments by the authors. It contains significant achievements with regards to the previously published papers (Modaressi and Laloui 1997; Laloui and Cekerevac 2003; Laloui and Cekerevac 2008a,b)

- The new proposed version offers a more advanced concept combining the efficiency of the isotropic thermoplastic mechanism and the capability of a Cam-clay family deviatoric mechanism enhanced by the bounding surface theory. As it is shown in this paper, the performance of the model is proved through significant numerical validations;
- This contribution provides all the needed detailed mathematical equations for the implementation in finite element codes; and
- Based on this new formulation of the model, it is now possible to extend it to more general aspects of environmental geomechanics, such as unsaturated conditions or time related effects.

First, some experimental observations of thermally-induced effects on soils are briefly shown in the light of elastothermoplasticity. Then, the state of the art on constitutive approaches in this field is presented and focus is made on the gradual improvement displayed by the successive constitutive models. A thermomechanical model is then introduced using a multimechanism plasticity concept. Finally, some selected comparisons between model simulations and experimental results for different combinations of thermomechanical loading paths are presented. Here, the considered temperature range is from 5 to 95 °C, which corresponds to that of the principal geoenvironmental applications concerned (without freezing or boiling of the pore water). This paper investigates the state of stress and strain in saturated soils due to heating, under the simplifying assumption that the influence of strain on the temperature field may be neglected.

Induced Thermal Effects

There are numerous experimental results available in the literature showing the influence of temperature on the behavior of soils. The most relevant results for the constitutive description of behavior will be considered here.

Soil Response to Heating-Cooling Cycles

Saturated soil is a two-phase material including a solid part (a skeleton of grains or particles surrounded by adsorbed water, for clays) and a fluid part (free water) in voids. For the considered temperature range, when a soil is heated, all of the components dilate. In the case of clayey soils, this dilation produces a decrease in the strength of the adsorbed layers and a modification of the

[1]Professor, Soil Mechanics Laboratory, Ecole Polytechnique Fédérale de Lausanne (EPFL), CH-1015 Lausanne, Switzerland. E-mail: lyesse.laloui@epfl.ch

[2]Researcher, Soil Mechanics Laboratory, Ecole Polytechnique Fédérale de Lausanne (EPFL), CH-1015 Lausanne, Switzerland (corresponding author). E-mail: bertrand.francois@epfl.ch

Note. This manuscript was submitted on March 4, 2008; approved on November 18, 2008; published online on March 5, 2009. Discussion period open until February 1, 2010; separate discussions must be submitted for individual papers. This paper is part of the ***Journal of Engineering Mechanics***, Vol. 135, No. 9, September 1, 2009. ©ASCE, ISSN 0733-9399/2009/9-932–944/$25.00.

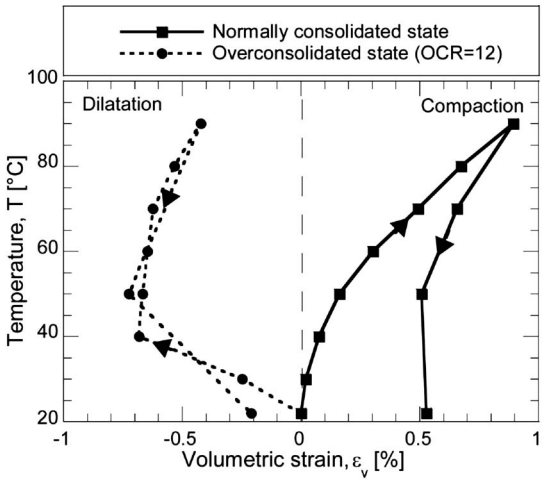

Fig. 1. Typical thermal behavior of kaolin clay during a thermal heating-cooling cycle at constant isotropic stress (Laloui and Cekerevac 2008b)

distance between the clay particles. This changes the equilibrium between the Van der Waals attractive forces and the electrostatic repulsive forces (Mitchell 1976), which result in one of the most characteristic thermal behaviors of clays. Under normally consolidated conditions (NC), the clay contracts when it is heated and a significant part of this deformation is irreversible upon cooling. This thermal contraction is an unusual behavior for any material (Fig. 1). During heating, the normally consolidated (NC) sample settles with a nonlinear volume variation. The behavior over the whole cycle indicates the irreversibility of strain due to thermal loading which is representative of thermal hardening. Even though there has been no physical change in effective stresses, this can be interpreted as the soil undergoing densification, i.e., overconsolidated behavior. The highly overconsolidated (OC) states produce mainly reversible dilation. Between these states, an intermediate one [low overconsolidation ratio (OCR)] first produces dilation, then a tendency toward contraction. The intensity of the reversible/irreversible parts of the deformation due to temperature cycling depends upon soil type and plasticity, in addition to stress level measured in terms of OCR (Cekerevac and Laloui 2004).

Thermal Effect on Compression Behavior

Preconsolidation pressure, p'_c, is considered here as the stress yield limit, which separates "elastic" preyield from "plastic" postyield behavior under isotropic or oedometric conditions. Several results from the literature show a decrease in the preconsolidation pressure with increasing temperature (Fig. 2).

For the considered temperature range, the isotropic and/or oedometric compressibilities of clayey materials before the yield point (elasticity) and after the yield point [normally consolidated line (NCL)—elastoplasticity] seem not to be affected by the temperature change, or at least the magnitude of variation of moduli remains negligible. Indeed, most experimental results have shown that NCL are almost parallel for different tested temperatures (Campanella and Mitchell 1968; Cekerevac and Laloui 2004).

Thermal Effect on Shear Strength

Until recently, the thermal effect on shear strength lacked confirmation. Some researchers concluded that heating caused a decrease in strength, while others reported slightly increased strength. Some experimental results are summarized by Cekerevac and Laloui (2004), which tend to confirm that the friction angle at critical state can either slightly increase or decrease with temperature.

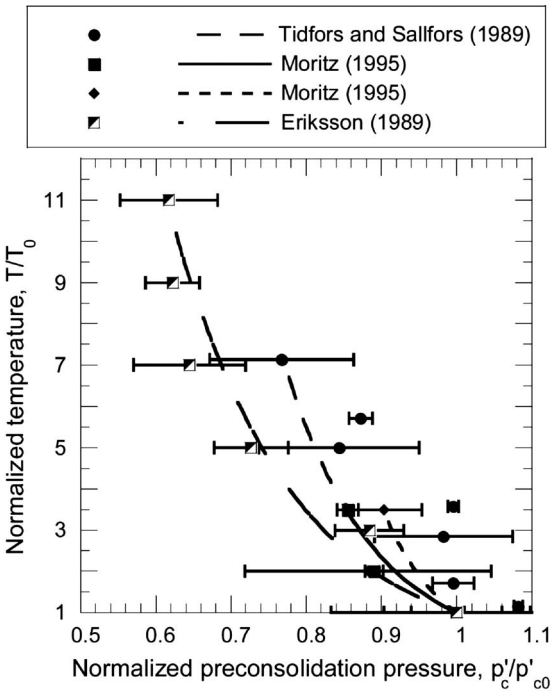

Fig. 2. Influence of temperature on the preconsolidation pressure (reported by Laloui and Cekerevac 2003) (Sources: Tidfors and Sällfors 1989; Mortiz 1995; Eriksson 1989)

Thermal Effect in Undrained Conditions

The higher thermal expansion of water than that of the solid skeleton induces pore water pressure increase when a saturated soil is heated under undrained conditions. Indeed, a temperature increase tends to enhance the pore space of the material proportionally to the thermal expansion coefficient of the solid skeleton. Nevertheless, this effect is more than counterbalanced by the thermal dilation of water. Moreover, when the soil tends to collapse during heating (due to thermoplastic behavior of NC soils), the undrained conditions make the decrease of pore space impossible, which provokes an additional increase in pore water pressure. Then, under undrained conditions, thermoelasticity, as well as thermoplasticity, results in excess pore water pressure when temperature increases. As a consequence, the effective mean stress tends to decrease by the same amount (Hueckel and Pellegrini 1992).

Relevant Contributions to the Thermomechanical Constitutive Modeling of Soils

The constitutive developments dealing with the thermomechanical behavior of saturated soils were investigated by the precursory works of Campanella and Mitchell (1968), wherein the mechanical response of soil along nonisothermal paths was interpreted by a means of constitutive relations. The volume change in drained conditions or the generated pore water pressure in undrained con-

ditions on nonisothermal paths were estimated through theoretical analyses based on the thermal dilatation coefficients of each soil constituent (water and solid), the repartition between phases (i.e., porosity), and the compressibility of water. In addition, the irreversible processes due to temperature were related to physicochemical structural adjustments.

Noting the lack of experimental data on the thermal effects on soils at the microscale, Hueckel and Borsetto (1990) proposed a macroscopic thermomechanical model based on phenomenological experiments. This model introduced thermoplasticity in addition to classical thermoelasticity of soil. Starting from a modified Cam-clay model (Roscoe and Burland 1968), the thermal shrinkage of the yield surface was introduced through the decrease of the preconsolidation pressure with temperature increase. The consistency equation had to be substantially adapted to consider temperature as a state variable. This work pioneered modern thermoplasticity constitutive modeling of fine-grained soils. However, some specific behavioral features were not fully reproduced by this precursory model. In particular, the irreversible thermal strain observed at intermediate degrees of surconsolidation (OCR) was not considered.

In the same vein, further developments were proposed by Modaressi and Laloui (1997), who started from an isothermal elastoplastic multimechanism model (Hujeux 1979) to develop a viscothermoplastic model that examines the decrease of the preconsolidation pressure with temperature. This matches with the concluding remarks of Hueckel and Borsetto (1990), who state that, for the sole mechanical part of soil behavior, a more sophisticated model should be chosen over the modified Cam-clay. Later, Laloui and Cekerevac (2003) enhanced this model by introducing a logarithmic expression for the evolution of preconsolidation pressure with temperature that required only one material parameter.

Aware of the need to improve the role of the OCR on the thermal expanding/contracting behavior in the aforementioned models, Cui et al. (2000) added a new thermal yield curve to allow for the generation of thermal irrecoverable strain, even at high OCR. As a consequence, the yield surface initially proposed by Hueckel and Borsetto (1990) was coupled with this new thermal yield limit.

This paper returns to the unique isotropic thermal yield surface and considers the thermal irrecoverable strains at the intermediate OCR by means of the bounding surface theory (Dafalias and Herrmann 1980), which allows for a progressive plasticity inside the external yield limit. This concept is closer to the real phenomenological behavior of the soil response. In that way, there is no distinction between mechanical and thermal hardenings. In the isotropic plane, both processes are described by a unique yield surface shrinking with temperature increase. Moreover, under mechanical loading, the bounding surface theory reproduces the transition between a fully elastic response and a total mobilization of the soil hardening very well.

ACMEG-T: Constitutive Model for the Elastothermoplastic Behavior of Soils

Advanced Constitutive Model for Environmental Geomechanics-Thermal effect (ACMEG-T) adopts multidissipative plasticity to develop the thermomechanical formulation. Due to the strain history dependence, the formulation is given in terms of infinitesimal increments. In the presence of a temperature field, the elastoplasticity principle (concept of a loading surface, f, in stress and temperature space, which limits the region of elastic deformation) allows that the total strain increment, $d\varepsilon_{ij}$, be split into thermoelastic, $d\varepsilon_{ij}^e$, and thermoplastic, $d\varepsilon_{ij}^p$, components

$$d\varepsilon_{ij} = d\varepsilon_{ij}^e + d\varepsilon_{ij}^p \tag{1}$$

Reference is made here to strains and stresses in the small deformation domain.

Thermohypoelasticity

$d\varepsilon_{ij}^e$ is the (i, j) strain increment component that does not modify the hardening state of the material. In all the paper, it will be understood that generic subscript notation of strain component ε_{ij} includes the shear strain components γ_{12}, γ_{13}, and γ_{23}, which are the conjugated variables of the shear stress components σ'_{12}, σ'_{13}, and σ'_{23} (see Appendix II).

Due to the reversible process, the hypoelastic constitutive part is not affected by the loading history of the material and is entirely defined by (Duhamel-Neumann equation)

$$d\varepsilon_{ij}^e = d\varepsilon_{ij}^{me} + d\varepsilon_{ij}^{Te} = E_{ijkl}^{-1} d\sigma'_{kl} - \beta_{T,ij} dT \tag{2}$$

where contraction is taken as positive. $d\sigma'_{kl}$ is the (k, l) component of the effective stress increment. $d\varepsilon_{ij}^{me}$ is the mechanically induced elastic strain increment and $d\varepsilon_{ij}^{Te}$ the thermally induced elastic strain increment. E_{ijkl} is the mechanical elastic tensor, which depends on the effective stress. $\beta_{T,ij}$ is the expansion coefficient vector, which depends on temperature, T. Considering an isotropic thermal dilatation, one can express the thermal coefficient as $\beta_{T,ij} = 1/3\beta'_s\delta_{ij}$ with β'_s being the volumetric thermal expansion coefficient of the solid skeleton and δ_{ij} Kronecker's symbol. The dependencies on the effective stress and the temperature enable nonlinear behavior of the elastic part. In the framework of elastothermoplasticity, Eq. (2) becomes

$$d\sigma'_{ij} = E_{ijkl}(d\varepsilon_{kl} - d\varepsilon_{kl}^{Te} - d\varepsilon_{kl}^{p}) \tag{3}$$

As shown in Eq. (2), the thermoelastic strain increment, $d\varepsilon_{ij}^e$, is composed of the superposition of a mechanical hypoelastic strain under adiabatic conditions increment, $d\varepsilon_{ij}^{me}$, and a reversible thermal strain increment, $d\varepsilon_{ij}^{Te}$. The volumetric and deviatoric parts are, respectively

$$d\varepsilon_v^e = d\varepsilon_v^{me} + d\varepsilon_v^{Te} = \frac{dp'}{K} - \beta'_s dT; \quad d\varepsilon_d^e = \frac{dq}{3G} \tag{4}$$

where ε_v^e=thermoelastic volumetric strain $(\varepsilon_v^e = \varepsilon_{11}^e + \varepsilon_{22}^e + \varepsilon_{33}^e)$ and ε_d^e=deviatoric elastic strain

$$\varepsilon_d^e = \frac{\sqrt{2}}{3}\left[(\varepsilon_{11}^e - \varepsilon_{22}^e)^2 + (\varepsilon_{22}^e - \varepsilon_{33}^e)^2 + (\varepsilon_{33}^e - \varepsilon_{11}^e)^2 + \frac{3}{2}(\gamma_{12}^{e2} + \gamma_{13}^{e2} + \gamma_{23}^{e2})\right]^{1/2} \tag{5}$$

q and p' are the deviatoric and effective mean stress, respectively, expressed as

$$q = \frac{\sqrt{2}}{2}[(\sigma'_{11} - \sigma'_{22})^2 + (\sigma'_{22} - \sigma'_{33})^2 + (\sigma'_{33} - \sigma'_{11})^2 + 6(\sigma'^2_{12} + \sigma'^2_{13} + \sigma'^2_{23})]^{1/2} \tag{6}$$

$$p' = (\sigma'_{11} + \sigma'_{22} + \sigma'_{33})/3 \tag{7}$$

An isotropic thermal dilatation of the solid skeleton is assumed. The volumetric thermal expansion coefficient, β'_s, increases with OCR and temperature

$$\beta'_s = [\beta'_{s0} + \zeta(T - T_0)]\xi \tag{8}$$

in which β'_{s0}=isotropic thermal expansion coefficient at a reference temperature, T_0 (usually ambient temperature), and ξ the ratio between the initial critical state pressure, p'_{cr0}, and the effective mean pressure, p', at ambient temperature

$$\xi = \frac{p'_{cr0}}{p'} \tag{9}$$

ζ corresponds to the slope of the variation of β'_s with respect to the current temperature, T, at $\xi=1$. The ζ dimension is $°C^{-2}$. Experimental evidence shows that this parameter (ζ) could be approximated by $[-\beta'_{s0}/100°C]$ (Laloui 1993). The hypoelastic moduli are given by

$$K = K_{\text{ref}}\left(\frac{p'}{p'_{\text{ref}}}\right)^{n^e}; \quad G = G_{\text{ref}}\left(\frac{p'}{p'_{\text{ref}}}\right)^{n^e} \tag{10}$$

where K_{ref} and G_{ref}=reference bulk and shear elastic moduli, respectively, at a reference pressure, p'_{ref} (the value of the effective mean pressure at which the reference hypoelastic moduli are measured); and n^e=material parameter.

Thermoplasticity

From Eq. (1), the thermoplastic strain increment can be expressed as the part of the total strain increment, which is not recoverable

$$d\varepsilon^p_{ij} = d\varepsilon_{ij} - d\varepsilon^e_{ij} \tag{11}$$

$$d\varepsilon^p_{ij} = d\varepsilon_{ij} + \beta_{T,ij}dT - E^{-1}_{ijkl}d\sigma'_{kl} \tag{12}$$

The particularity of the present model is that the total strain increment induced by plasticity (hardening of the material) is a linear combination of two irreversible processes (isotropic as well as deviatoric). Therefore, the total plastic strain increment, $d\varepsilon^p_{ij}$, is the sum of "partial" plastic strain increments, $d\varepsilon^{p,k}_{ij}$, induced by each of the two processes (mechanisms) k

$$d\varepsilon^p_{ij} = \sum_{k=1}^{2} d\varepsilon^{p,k}_{ij} \tag{13}$$

These considerations result from the theory of multimechanism plasticity (Koiter 1960; Mandel 1965; Hujeux 1979). Each dissipative process is described through an evolution law activated by a yield function, through a dissipative potential and through a plastic multiplier (Rizzi et al. 1996). Each mechanism is activated if the stress state reaches the yield function corresponding to the considered mechanism: f_{iso} and f_{dev} for the isotropic and deviatoric mechanisms, respectively. This activation creates irreversible strain and the total plastic strain increment can be expressed as

$$d\varepsilon^p_{ij} = \sum_{k=1}^{2} \lambda^p_k \frac{\partial g_k}{\partial \sigma'_{ij}} \tag{14}$$

where g_k=plastic potentials corresponding to each mechanism and λ^p_k=plastic multipliers, which are positive if the corresponding mechanism is activated ($f_k=0$ and $df_k=0$), otherwise they are null.

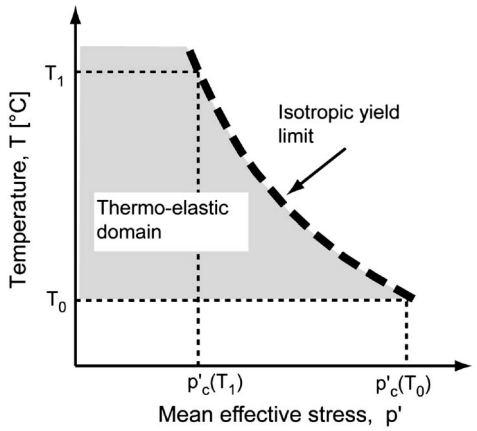

Fig. 3. Isotropic thermoplastic yield limit

Then, with this multimechanism concept, the two yield functions define a closed domain in the effective stress and temperature space inside which the behavior of the material is reversible. In the following sections, yield functions, plastic potentials and the procedure to determine plastic multipliers are introduced for each mechanism.

Isotropic Thermoplastic Mechanism

The yield limit, f_{iso}, of the isotropic thermoplastic mechanism is represented in the effective mean stress p'-temperature T plane (Fig. 3) and is expressed by

$$f_{\text{iso}} = p' - p'_c r_{\text{iso}} \tag{15}$$

In this equation, the parameter r_{iso} corresponds to the degree of plastification (mobilized hardening) of the isotropic yield limit. This enables a progressive evolution of the isotropic yield limit

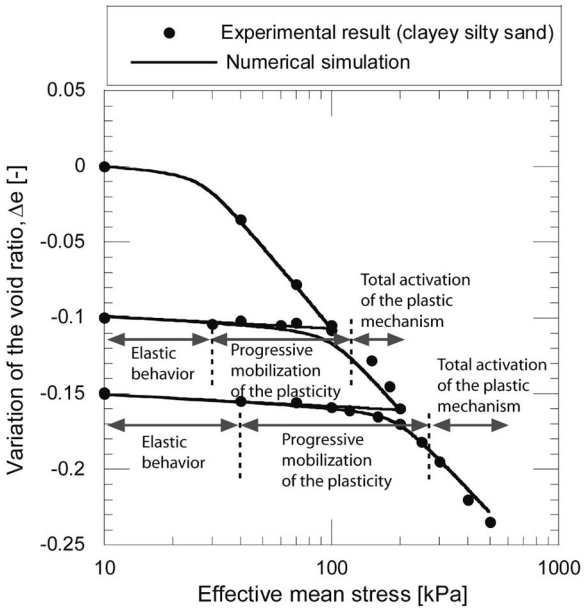

Fig. 4. Isotropic compression test: comparison of experimental results (Jamin 2003) and a numerical simulation using the bounding surface theory

during loading and a partial comeback of this limit during unloading. The introduction of this parameter is motivated by the need for an accurate description of the loading-unloading stress-strain evolution. Typical isotropic compression experimental results on a remolded soil, as shown in Fig. 4, clearly show progressive mobilization of the plasticity before reaching the virgin consolidation line. Thus, this hardening parameter, r_{iso}, whose evolution is governed by the consistency condition, transforms the well-known bilinear compression behavior in the void ratio log of the effective mean pressure ($e-\ln p'$) plane into a smoother curve, as observed experimentally. Dafalias and Herrmann (1980) introduced this concept, termed the bounding surface theory. The basic idea of this approach is that plastic deformation may occur when the stress state lies on or within the bounding surface (e.g., external surface), by allowing the plastic modulus to be a decreasing function of the distance of the stress state from a corresponding point on the bounding surface.

During loading, r_{iso} is a hyperbolic function of the plastic volumetric strain induced by the isotropic mechanism, $\varepsilon_v^{p,iso}$ (Hujeux 1979)

$$r_{iso} = r_{iso}^e + \frac{\varepsilon_v^{p,iso}}{c + \varepsilon_v^{p,iso}} \quad \text{and} \quad dr_{iso} = \frac{(1 - r_{iso})^2}{c} d\varepsilon_v^{p,iso} \tag{16}$$

where c=material parameter.

During unloading, r_{iso} decreases to follow the decrease of effective mean pressure, p', and at reloading, at the moment of change of direction of solicitation (unloading-reloading), r_{iso} is adjusted to keep a defined elastic nuclei (r_{iso}^e)

$$r_{iso} = r_{iso}^e + \frac{p'_{cyc}}{p'_c} + \frac{\varepsilon_v^{p,cyc,iso}}{c + \varepsilon_v^{p,cyc,iso}} \leq 1 \tag{17}$$

where p'_{cyc}=effective mean stress at the last change of direction of solicitation (unloading-reloading) and $\varepsilon_v^{p,cyc,iso}$=volumetric plastic strain produced by the isotropic mechanism since this change of direction of solicitation.

The behavior of the isotropic mechanism on an isotropic loading-unloading-reloading path is explained and illustrated in Appendix I.

The preconsolidation pressure, p'_c, is expressed as a function of the volumetric plastic strain, ε_v^p, and the temperature

$$p'_c = p'_{c0} \exp(\beta \varepsilon_v^p) \tag{18}$$

where p'_{c0}=value of the initial preconsolidation pressure at temperature T; and β=plastic compressibility modulus (the slope of the linear function $\varepsilon_v^p - \log p'_c$). A dependency law for the thermal evolution of the preconsolidation pressure, p'_{c0}, is introduced to take into account the thermal effect on the yield limit (Laloui and Cekerevac 2003)

$$p'_{c0} = p'_{c0T0}[1 - \gamma_T \log(T/T_0)] \tag{19}$$

where p'_{c0T0}=initial value of the preconsolidation pressure at the reference temperature, T_0; and γ_T=material parameter. The expression of the isotropic thermoplastic yield limit is, thus, given by

$$f_{iso} = p' - p'_{c0T0} \exp\{\beta \varepsilon_v^P\}[1 - \gamma_T \log(T/T_0)] r_{iso} \tag{20}$$

Eq. (20) contains three material parameters: β and c (contained in r_{iso}), expressing the evolution of mechanical hardening, and γ_T, controlling the evolution of thermal hardening.

The flow rule is associated ($f_{iso}=g_{iso}$)

$$d\varepsilon_{ii}^{p,iso} = \lambda_{iso}^p \frac{\partial g_{iso}}{\partial \sigma'_{ii}} = \frac{\lambda_{iso}^p}{3} \tag{21}$$

The plastic multiplier of the isotropic mechanism, λ_{iso}^p, is determined using Prager's consistency equation (Prager 1958), as presented below.

The behavior of the isotropic mechanism on a heating path is illustrated in Fig. 5. According to the degree of consolidation of the material, heating can induce dilatation (elasticity for high OCR, Case C), compaction (elastothermoplasticity, Case A) or transitional behavior (elasticity followed by elastothermoplasticity, Case B). The three main parameters governing this mechanical response on nonisothermal paths are r_{iso}^e, c γ_T, and β, controlling the size of elastic nuclei of the isotropic mechanism, the rate of plasticity inside the bounding surface, the shape of the isotropic yield limit in the ($T-p'$) plane and the plastic compressibility, respectively.

Deviatoric Thermoplastic Mechanism

The deviatoric yield limit is an extension of the original Cam-clay model (Roscoe and Burland 1968; Hujeux 1979)

$$f_{dev} = q - Mp'\left(1 - b \ln \frac{p'd}{p'_c}\right) r_{dev} = 0 \tag{22}$$

where b=material parameter defining the shape of the deviatoric yield limit and d=ratio between the preconsolidation pressure, p'_c, and the critical pressure, p'_{cr}. M=slope of the critical state line in the ($q-p'$) plane

$$M = \frac{6 \sin \phi'}{3 - \sin \phi'} \tag{23}$$

where ϕ'=friction angle at critical state. As shown by (Cekerevac and Laloui 2004), the friction angle may depend on temperature. So, the following expression is proposed (Laloui 1993):

$$M = M_0 - g(T - T_0) \tag{24}$$

where M_0=slope of the critical state line at ambient temperature T_0 and g=average slope of variation of friction angle at critical state with temperature.

r_{dev}, in the same way as for the isotropic mechanism, is the degree of plastification of the deviatoric mechanism and also enables a progressive evolution of the deviatoric yield limit during loading

$$r_{dev} = r_{dev}^e + \frac{\varepsilon_d^p}{a + \varepsilon_d^p} \quad \text{and} \quad dr_{dev} = \frac{(1 - r_{dev})^2}{a} d\varepsilon_d^p \tag{25}$$

where r_{dev}^e and a=material parameters defining the size of the elastic nuclei of the deviatoric mechanism and the evolution of r_{dev}, respectively, while ε_d^p=deviatoric plastic strain.

Through a combination of the previous equations, the deviatoric yield surface (Eq. (22)) becomes, under nonisothermal conditions (Fig. 6)

$$f_{dev} = q - r_{dev} p'[M_0 - g(T - T_0)] \times \left\{1 - b \ln \frac{dp'}{p'_{c0T0} \exp(\beta \varepsilon_v^p)[1 - \gamma_T \log(T/T_0)]}\right\} = 0 \tag{26}$$

The hardening and dilatancy rules are the following:

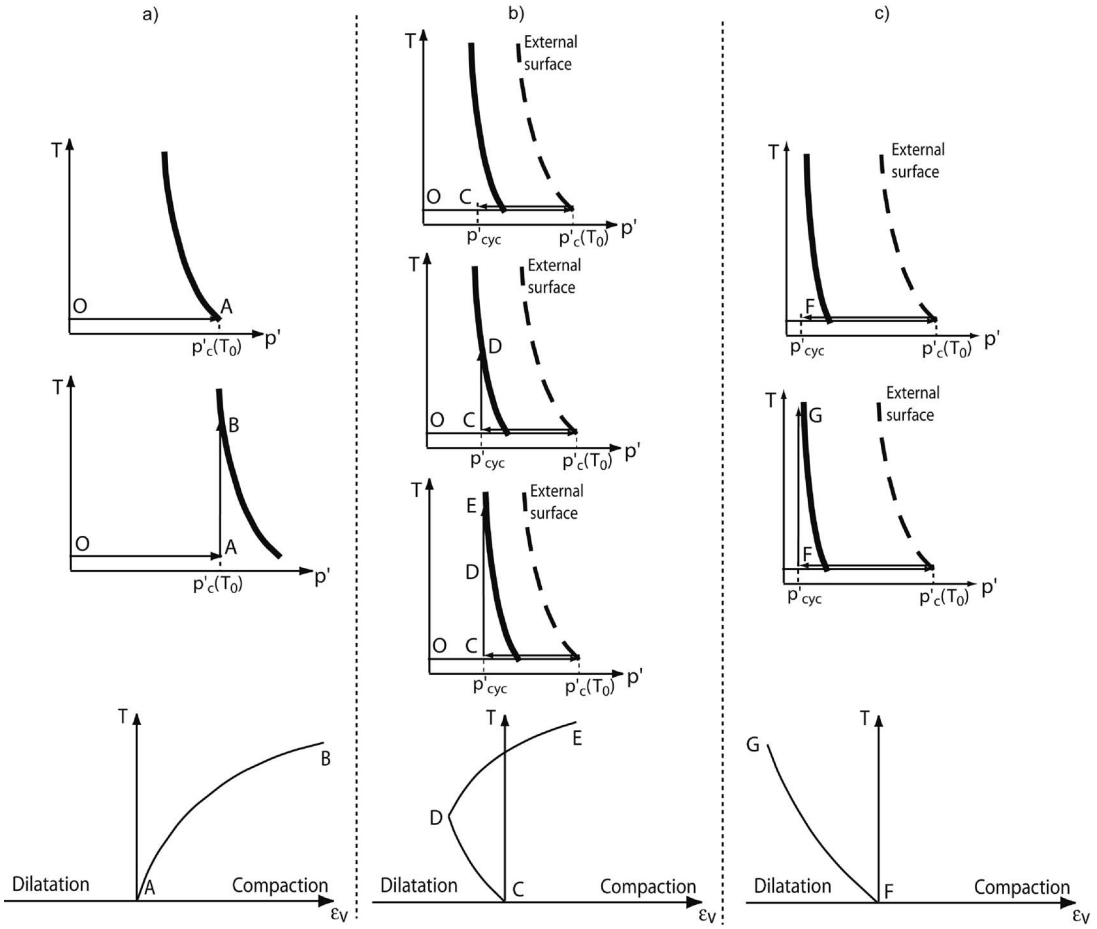

Fig. 5. Qualitative explanation of the response of the isotropic thermoplastic mechanism under heating at different degrees of consolidation: (a) normally consolidated; (b) slightly overconsolidated; and (c) highly overconsolidated

$$d\varepsilon_{ij}^{p,\mathrm{dev}} = \lambda_{\mathrm{dev}}^{p}\frac{\partial g_{\mathrm{dev}}}{\partial \sigma'_{ij}} = \lambda_{\mathrm{dev}}^{p}\frac{1}{Mp'}\left[\frac{\partial q}{\partial \sigma'_{ij}} + \alpha\left(M - \frac{q}{p'}\right)\frac{1}{3}\delta_{ij}\right] \tag{27}$$

$$\text{with}\quad \frac{\partial q}{\partial \sigma'_{ij}} = \begin{cases} \dfrac{3}{2q}(\sigma'_{ij} - p') & \text{if } i = j \\ \dfrac{3\sigma'_{ij}}{q} & \text{if } i \neq j \end{cases} \tag{28}$$

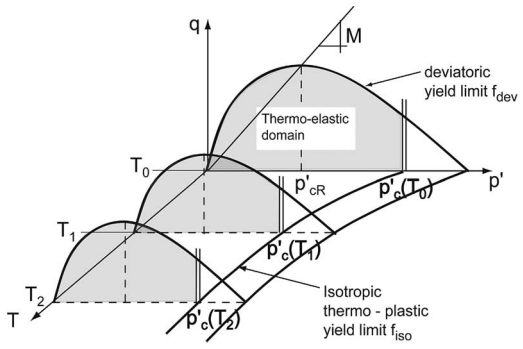

Fig. 6. Coupled thermoplastic yield limits

$$d\varepsilon_{v}^{p,\mathrm{dev}} = \lambda_{\mathrm{dev}}^{p}\frac{\partial g_{\mathrm{dev}}}{\partial p'} = \lambda_{\mathrm{dev}}^{p}\frac{\alpha}{Mp'}\left[M - \frac{q}{p'}\right] \tag{29}$$

$$d\varepsilon_{d}^{p} = \lambda_{\mathrm{dev}}^{p}\frac{\partial g_{\mathrm{dev}}}{\partial q} = \lambda_{\mathrm{dev}}^{p}\frac{1}{Mp'} \tag{30}$$

where α = material parameter introducing the nonassociative behavior. The plastic multiplier, $\lambda_{\mathrm{dev}}^{p}$, must be determined, as well as the isotropic mechanism, using Prager's consistency condition (Prager 1958).

Coupling between the Two Mechanisms

The isotropic and the deviatoric yield limits are coupled through the hardening variable, ε_v^p. Indeed, the preconsolidation pressure, p'_c, which depends on ε_v^p [Eq. (18)], appears in the expression of the two yield limits. Therefore, if ε_v^p increases due to the activation of one of the mechanisms, the yield limit of the other mechanism will also move. As a consequence, the two plastic multipliers ($\lambda_{\mathrm{iso}}^{p}$ and $\lambda_{\mathrm{iso}}^{p}$) are related.

When the two mechanisms are activated simultaneously, the total volumetric plastic strain increment, $d\varepsilon_v^p$, is the sum of the volumetric plastic strain increments due to each mechanism [Eqs. (21) and (29)]

$$d\varepsilon_v^p = \lambda_{\text{dev}}^p \frac{\partial g_{\text{dev}}}{\partial p'} + \lambda_{\text{iso}}^p \frac{\partial g_{\text{iso}}}{\partial p'} = \lambda_{\text{dev}}^p \frac{\alpha}{Mp'}\left[M - \frac{q}{p'}\right] + \lambda_{\text{iso}}^p \quad (31)$$

The two consistency conditions must be met simultaneously, leading to the solving of two equations with two unknowns (Rizzi et al. 1996)

$$\mathbf{dF} = \frac{\partial \mathbf{F}}{\partial \boldsymbol{\sigma}'}:d\boldsymbol{\sigma}' + \frac{\partial \mathbf{F}}{\partial T}\,.\,dT + \frac{\partial \mathbf{F}}{\partial \boldsymbol{\pi}}\,.\,\frac{\partial \boldsymbol{\pi}}{\partial \boldsymbol{\lambda}^{\mathbf{p}}}\,.\,\boldsymbol{\lambda}^{\mathbf{p}}$$
$$= \mathbf{s}:d\boldsymbol{\sigma}' + \mathbf{t}\,.\,dT - \mathbf{H}\,.\,\boldsymbol{\lambda}^{\mathbf{p}} \le 0; \quad \boldsymbol{\lambda}^{\mathbf{p}} \ge 0; \quad \mathbf{dF}\,.\,\boldsymbol{\lambda}^{\mathbf{p}} \ge 0 \quad (32)$$

where $\boldsymbol{\sigma}'$=stress vector and $\boldsymbol{\pi}$=internal variables. $\mathbf{s}$ collects the stress gradients and $\mathbf{t}$ the temperature gradient of the loading function $\mathbf{F}$. $\mathbf{H}$ is the matrix of hardening moduli $H_{\alpha\beta}=-\partial f_\alpha / \partial \lambda_\beta^p$, $\boldsymbol{\lambda}^{\mathbf{p}}$ is the plastic multiplier vector and $\mathbf{dF} \le 0$ expresses Prager's consistency condition (Prager 1958) extended to multiple dissipation processes.

The isotropic and deviatoric yield functions, f_{iso} and f_{dev}, both count two internal variables, r_{iso} and ε_v^p, for the isotropic yield function and r_{dev} and ε_v^p for the deviatoric yield function. Appendix II addresses the development of Eq. (32) to express the consistency equations with respect to the internal variables and to express the stress increment response with respect to prescribed strain increment.

Undrained Conditions

The experimental evidence presented in the section "Thermal effect in undrained conditions" clearly shows that the undrained nonisothermal behavior of soils must be addressed by means of a two-phase approach. In this context, three distinct thermal expansion coefficients must be considered, i.e., the water, the grain and the solid skeleton thermal expansion coefficients, β_w', β_{sG}', and β_s', respectively. β_w' is implemented according to the linear thermal dependency proposed by Campanella and Mitchell (1968) with $\beta_w'(22\,^\circ\text{C}) = 2.73\ 10^{-4}\,^\circ\text{C}^{-1}$ and $\beta_w'(80\,^\circ\text{C}) = 6.27\ 10^{-4}\,^\circ\text{C}^{-1}$.

The nonisothermal mass conservation equations of the two-phase soil can be expressed as follows with the assumption of incompressible grains (Lewis and Schrefler 1987):

$$n\beta_w dp_w = [n\beta_w' + (1-n)\beta_{sG}']dT + d\varepsilon_v \quad (33)$$

where β_w=water compressibility and n=porosity. By combining Eqs. (1), (4), and (31), Eq. (33) results in the expression of pore water variation

$$dp_w = \frac{[n\beta_w' + (1-n)\beta_{sG}' - \beta_s']dT + \dfrac{dp'}{K} + \lambda_{\text{dev}}^p \dfrac{\alpha}{Mp'}\left[M - \dfrac{q}{p'}\right] + \lambda_{\text{iso}}^p}{n\beta_w} \quad (34)$$

Being under undrained conditions, the effective mean stress increment, dp', must be deduced from the total mean stress increment, dp, and the pore water pressure increment, dp_w, through the expression of Terzaghi's effective stress ($dp' = dp - dp_w$). Finally, the increment of pore water pressure generated by any thermomechanical load is equal to

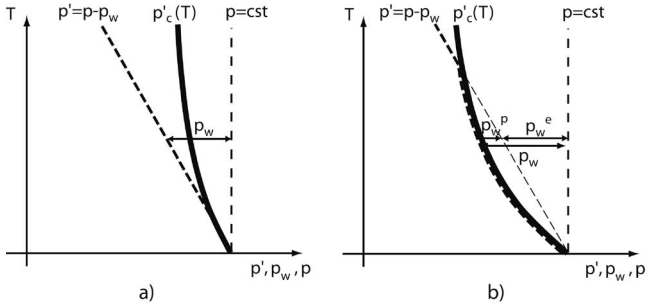

Fig. 7. Schematic representation of the evolution of pore water pressure and effective mean stress when a normally consolidated soil is heated: (a) the effective mean stress decreases faster than the yield limit—elastic behavior; (b) the effective mean stress decreases more slowly than the yield limit—elastoplastic behavior

$$dp_w = \frac{[n\beta_w' + (1-n)\beta_{sG}' - \beta_s']dT + \dfrac{dp}{K} + \lambda_{\text{dev}}^p \dfrac{\alpha}{M(p-p_w)}\left[M - \dfrac{q}{p-p_w}\right] + \lambda_{\text{iso}}^p}{n\beta_w + (1/K)} \quad (35)$$

It should be mentioned that the determination of plastic multipliers, λ_{dev}^p and λ_{iso}^p, requires the use of the effective mean stress increment, which also implies knowledge of the pore water pressure increment. This results in the fact that the calculation of pore water pressure variation involving elastothermoplasticity requires an iterative procedure.

This concept of elastothermoplasticity under undrained conditions can be illustrated by the undrained heating of a NC soil. Under drained conditions, Fig. 5(a) shows that the shrinkage of the isotropic yield limit induced by temperature increase results in thermal collapse of the soil. Under undrained conditions, the temperature increase produces pore water pressure. Then, at constant total stress, it reduces the effective mean stress. As a result, on the one hand, the yield limit decreases; however, on the other hand, the effective mean stress also decreases. Thus, as shown in Fig. 7, two cases may appear. If the effective mean stress decreases (due to pore water increase) faster than the isotropic yield limit [due to the decrease in preconsolidation pressure, Eq. (19)], the process is elastic [i.e., the plastic multipliers λ_{dev}^p and λ_{iso}^p are equal to zero in Eq. (35)] [Fig. 7(a)]. On the contrary, if the effective mean stress decreases more slowly than the isotropic yield limit, the stress point reaches the yield limit, which activates the isotropic mechanism. Plasticity is then induced. However, due to the fact that the hardening process could not occur under undrained conditions, additional pore water pressure, p_w^p, is generated to maintain the stress point on the isotropic yield surface [Fig. 7(b)].

The fact that the variation of the effective mean stress could be faster or slower than the isotropic yield limit variation mainly depends on the soil type, represented by the material parameter, γ_T.

Validation of the Constitutive Model

As a numerical validation of the ACMEG-T constitutive model, thermomechanical experimental results on Bangkok clay under drained and undrained conditions are used (Abuel-Naga et al. 2006, 2007).

Table 1. Model Parameters for the Simulation of the Thermomechanical Response of Bangkok Clay

Elastic parameters		
K_{ref}, G_{ref}, n^e, β'_{s0}, β'_{sG}	[MPa], [MPa], [−], [°C^{-1}], [°C^{-1}]	42, 15, 1, 2.10^{-4}, 2.10^{-4}
Isotropic plastic parameters		
β, γ_T, c, r^e_{iso}	[−], [−], [−], [−]	5.49, 0.52, 0.04, 0.15
Deviatoric plastic mechanical parameters		
b, d, ϕ'_0, g, α, a, r^e_{dev}	[−], [−], [°], [−], [−], [−], [−]	0.2, 1.6, 22.66, 1.10^{-3}, 2, 0.02, 0.1

Parameter Determination

The model parameters were determined using a minimum amount of tests. Thus, two isotropic compression tests performed at two constant temperatures (25 and 90°C) were used to establish the isotropic parameters K_{ref}, β, γ_T, and c. The determination of the compressibility indexes (κ and λ) of these curves enables the reference bulk elastic modulus, K_{ref}, and the plastic compressibility modulus to be obtained easily using the following expressions:

$$K_{ref} = \frac{1+e_0}{\kappa} p'_{ref}; \quad \beta = \frac{1+e_0}{\lambda - \kappa} \tag{36}$$

where p'_{ref}=reference effective mean pressure for which K_{ref} is defined (p'_{ref}=1 MPa in the present case) and e_0 is the initial void ratio for which both parameters are established. The slope of the logarithmic decrease of the preconsolidation pressure with temperature, γ_T, is evaluated by comparing the values of effective mean pressures corresponding to the inflection point of the compression curves (e.g., the preconsolidation pressure) obtained at 25°C (p'_{cT0}) and 90°C (p'_{cT1})

$$\gamma_T = \frac{1 - \frac{p'_{cT1}}{p'_{cT0}}}{\log\left(\frac{T_1}{T_0}\right)} \tag{37}$$

Finally, the parameter c is determined by curve fitting to obtain the best transition between elastic and elastoplastic isotropic behavior. The thermoelastic parameter, β'_{s0}, has been calculated using the quantification of the volumetric strain induced by a heating test on a highly overconsolidated soil (p'_c=25 kPa and OCR=8).

The deviatoric parameters, G_{ref}, b, d, ϕ'_0, α, and a, have been determined using one triaxial test at ambient temperature. The determination of the slope of the critical state line M_0 requires only one triaxial test

$$M_0 = \frac{q_{cr}}{p'_{cr}} \tag{38}$$

where q_{cr} and p'_{cr}=deviator stress and the effective mean pressure at the critical state (e.g., when $\partial q/\partial \varepsilon_{11}=0$ and $\partial \varepsilon_v/\partial \varepsilon_{11}=0$, ε_{11} being the axial strain).

The parameter d can be deduced through the plastic compressibility parameter, β, and the total volumetric plastic strain produced during the test, ε^p_v

$$d = \frac{p'_{c0}\exp(\beta \varepsilon^p_v)}{p'_{cr}} \tag{39}$$

where ε^p_v is unknown but can be obtained by subtracting the volumetric elastic strain, ε^e_v, from the total measured volumetric strain, ε_v

$$\varepsilon^p_v = \varepsilon_v - \varepsilon^e_v = \varepsilon_v - \frac{\Delta p'}{K} = \varepsilon_v - \left(\frac{p'_{ref}}{p'}\right)^{n^e} \frac{\Delta p'}{K_{ref}} \tag{40}$$

The three other deviatoric parameters, b, α, and a, have been determined by curve fitting. Finally, the temperature influence on the friction angle, g, has been determined by comparing friction angle values at 25 and 90°C. The slope of the critical state line at 90°C, M_1, can be compared with M_0 to deduce g

$$g = \frac{M_0 - M_1}{T_1 - T_0} \tag{41}$$

All of these parameters are summarized in Table 1.

Drained Simulations

Numerical simulations of drained compression tests at three different temperatures are shown in Fig. 8. It is useful to notice that two of the experimental results (at 25 and 90°C) have been used to determine isotropic parameters and, therefore, are back-predictions, while the test at 70°C is a blind simulation. Fig. 9 shows the comparison between the predicted and experimental results on a combined thermomechanical path. The test consists in oedometric loading in a normally consolidated state until a effective vertical stress of 100 kPa, followed by a thermal cycle (25-90-25°C) and finishing with vertical loading up to 200 kPa. Fig. 10 shows experimental and numerical results on heating-cooling cycles for different OCRs (OCR=8, 4, 2, and 1). The test for the higher OCR was used to determine the thermal dilatation coefficient on the cooling path that is purely thermoelastic. The other numerical results are blind predictions. Figs. 8–10 clearly show good agreement between the numerical predictions of

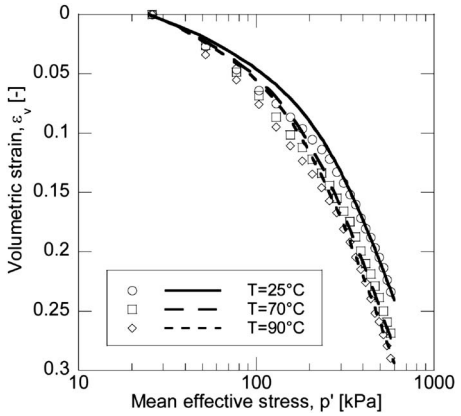

Fig. 8. Numerical simulations of isotropic compression tests at three different temperatures. Points: experimental results; lines: numerical simulations.

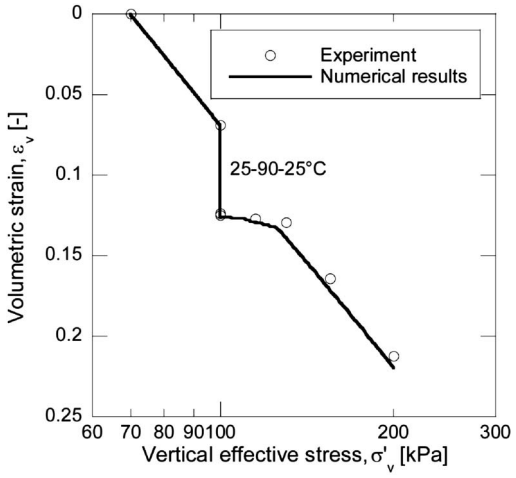

Fig. 9. Numerical simulations of a combined thermomechanical oedometric path. Comparison with experimental results.

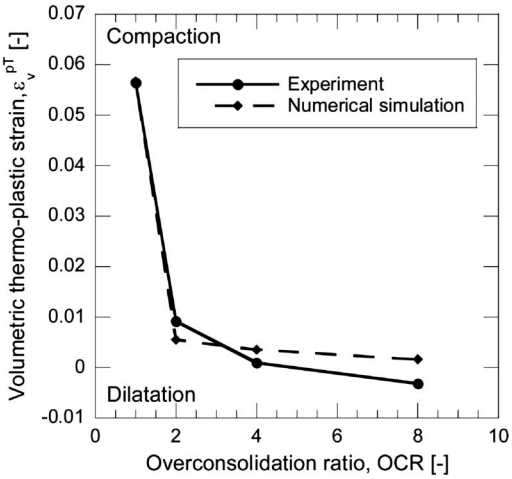

Fig. 11. Effect of OCR on the mechanical response of Bangkok clay along a heating-cooling cycle. Comparison between numerical simulations and experiments.

ACMEG-T and experimental results on thermomechanical isotropic paths. Moreover, the strain induced by each thermal cycle in Fig. 10 (e.g., thermoplastic strain) is given with respect to the OCR in Fig. 11. This underlines the capability of the model to consider the great dependence of the stress history on the thermoplastic-induced strain.

Numerical simulations of drained triaxial tests at three different constant temperatures for initially normally consolidated states have been performed and are compared with experimental results in Fig. 12. These results clearly show the thermal strengthening of the material, which results in an increase in strength of about 25% for a thermal gradient of 70°C. Such an effect is well reproduced by the numerical simulations.

Undrained Simulations

The numerical simulations of induced pore water pressure for undrained heating-cooling cycles at three different stress states (i.e., OCR) are shown in Fig. 13 and are compared with experimental results.

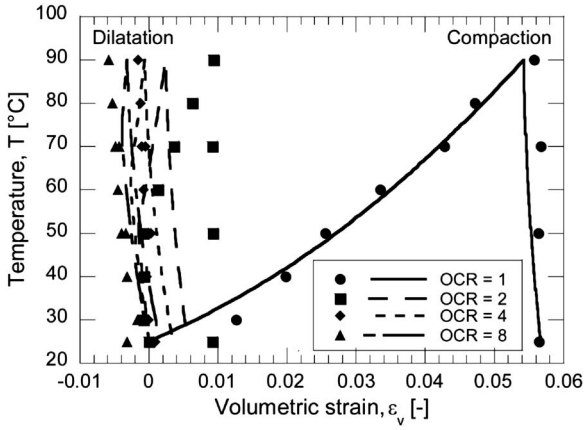

Fig. 10. Numerical simulations of a heating-cooling cycle at different degrees of consolidation under oedometric conditions (vertical preconsolidation pressure=200 kPa). Points: experimental results; lines: numerical simulations.

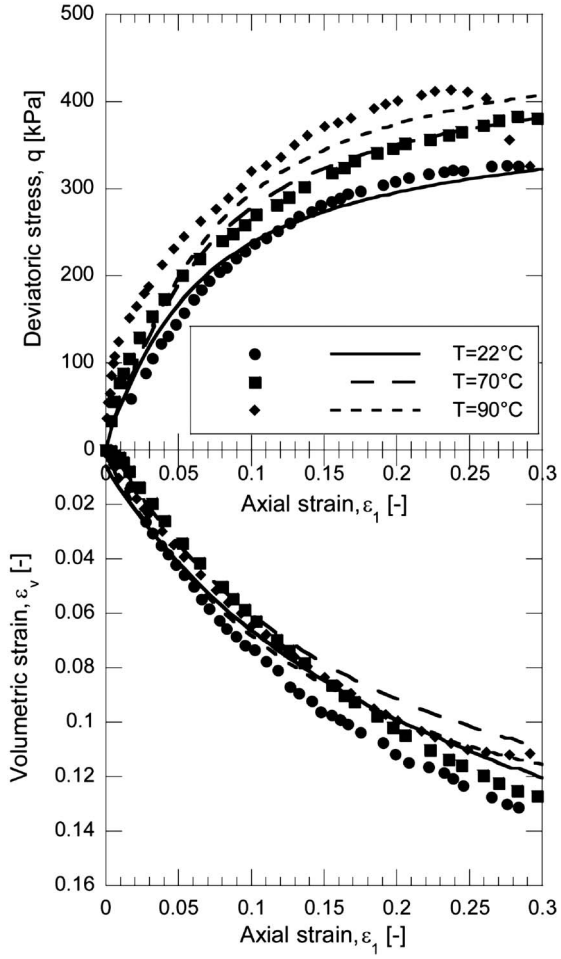

Fig. 12. Numerical simulations of drained triaxial compression tests on normally consolidated Bangkok clay (p'_c=200 kPa). Points: experimental results; lines: numerical simulations.

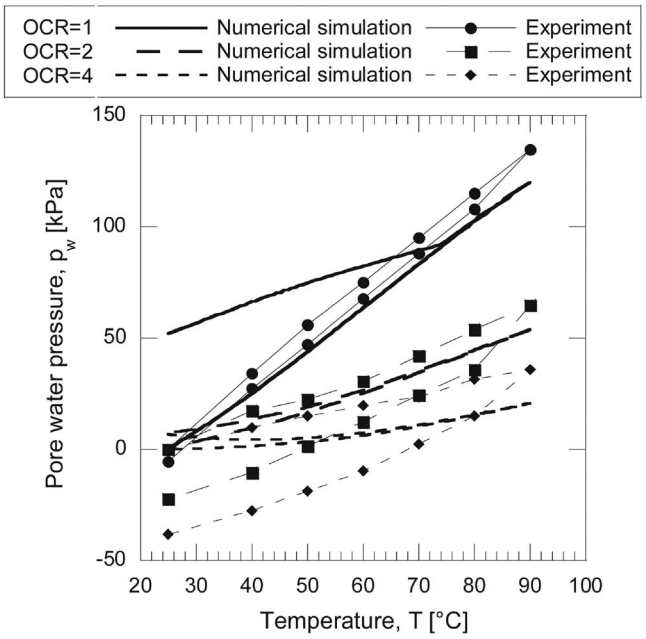

Fig. 13. Numerical simulations of undrained heating-cooling cycles at different degrees of consolidation under oedometric conditions (vertical preconsolidation pressure=200 kPa). Points: experimental results; lines: numerical simulations.

On the heating paths, the ACMEG-T computations fit very well with the experimental points. The soil response is purely elastic for any OCR. As explained in section "Undrained conditions," this corresponds to a faster decrease in effective mean stress than the shrinkage of the isotropic yield surface with temperature [Fig. 7(a)]. Thus, the induced pore water pressure is only governed by the first term of Eq. (35). The nonlinearity of the curve is due to the evolution of the bulk moduli and of the thermal expansion coefficients of the solid skeleton and water with stress state and/or temperature [Eqs. (8) and (10), and $\beta_f'(T)$, respectively].

On the cooling paths, the numerical predictions exhibit almost reversible behavior for overconsolidated states, while irrecoverable positive pore water pressure is generated for the normally consolidated state. This irreversible response provided by the ACMEG-T model occurs during the decrease in pore water pressure (i.e., the increase of the effective mean stress), which is equivalent to a mechanical load. Because the model used the bounding surface theory, this effective mean stress increase may produce plastic strain, even if the stress state lies within the external yield surface. At this cooling stage, the experimental points slightly differ from the numerical predictions.

Let's remarks that the very small irreversibilities observed for the overconsolidated states are not related to plastic processes but are due to the nonlinear elasticity and the integration method which always considers the rigidity corresponding to the effective stress at the end of the time step. Finally, it is worth to notice that the isotropic plastic mechanism is not validated here under undrained heating phase because of the thermoelastic response observed on this path [Fig. 7(a)].

Discussion of Numerical Predictions

This set of numerical simulations of the thermomechanical response of a clay along isotropic and deviatoric paths under drained and undrained conditions compares well with the experiments. In particular, the thermoplasticity brings substantial advancements in the predictions of the mechanical response of soils at various temperatures. If thermoplasticity had been neglected, the numerical simulation of Figs. 8, 10, and 12 would have been unaffected by the temperature of the test.

Moreover, it has been shown that, with very few experimental tests, the thermomechanical model parameters can be determined. Indeed, only two isotropic compression tests, one heating test on a highly overconsolidated sample and two drained triaxial tests at two different temperatures, are needed to get the whole set of model parameters. In other words, based on only five test results, the constitutive model is able to reproduce the mechanical response of soils on any complex thermomechanical path under drained and undrained conditions.

Conclusions

The main effects of temperature on the mechanical behavior of saturated cohesive soils have been reviewed based on experimental evidence. These experimental observations clearly demonstrate the important role of thermoplastic effects in the thermomechanical response of soils. The modeling of the mechanical behavior under nonisothermal conditions requires advanced elastothermoplastic stress-strain frameworks. In that context, the elastoplasticity and the critical state theory helps to offer a constitutive framework able to reproduce these thermomechanical features of behavior. In the continuation of the developments in the field, this model brings noticeable advancement thanks to the simplification of the definition of the thermomechanical yield surface in the isotropic plane. This unique surface considers not only the thermoplasticity observed at low and intermediate OCRs, but also the plasticity under mechanical loading. Consequently, the model consistency makes easy its implementation in finite element codes. Also, it provides a strong structure on which additional environmental variables may be integrated, such as suction or time related effects.

The ACMEG-T constitutive equations have been addressed using the concepts of multimechanism and bounding surface theory. Nonlinear thermoelasticity, joined with two coupled thermoplastic processes, isotropic and deviatoric, have been used in a unified framework. Both mechanisms are coupled through the volumetric plastic strain governing the evolution of the preconsolidation pressure as the key model variable. Each dissipative mechanism has been described by a yield function, a dissipative potential and a plastic multiplier in agreement with Prager's consistency equations.

Analytical relations to determine the model parameters have been presented. Finally, the proposed model has been validated by predictions of experimental results on a clay. This set of numerical simulations has shown that ACMEG-T is able to reproduce the mechanical response of soils on any complex thermomechanical path under drained and undrained conditions using only five test results to calibrate material parameters.

Therefore, ACMEG-T constitutes a performing constitutive tool to model geomechanical problems governed by highly coupled thermomechanical processes, such as high-level nuclear waste disposal or energy foundations.

Acknowledgments

This work was partially funded by the Swiss State Secretariat for Education and Research SER, Grant No. OFES C04.0021.

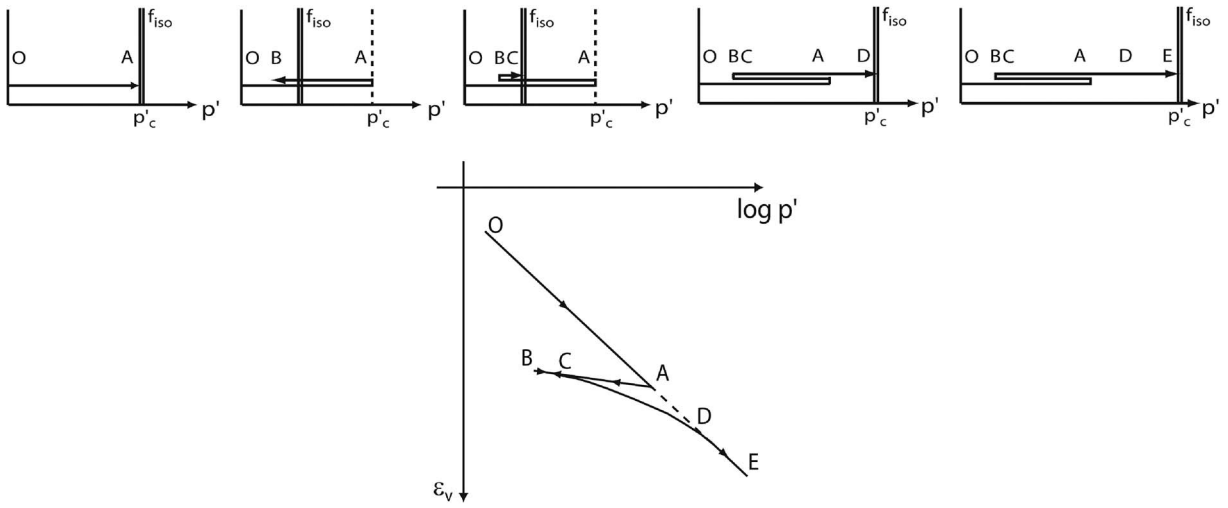

Fig. 14. Schematic behavior of the isotropic plastic mechanism over a mechanical isotropic loading-unloading-reloading cycle

Appendix I. Behavior of the Isotropic Mechanism

On an isotropic loading-unloading-reloading path, Fig. 14 presents the isotropic mechanism response schematically. During the first loading (O-A, the initial yield limit being in O), conventional hardening of the yield surface occurs [$r_{\text{iso}}=1$; $d\varepsilon_v^p>0$, p_c' increases following Eq. (18)]. The unloading (A-B) takes place elastically and so does not produce plastic strain ($d\varepsilon_v^p=0$, p_c' remains constant). The first part of the reloading (B-C) takes place inside the elastic nuclei ($r_{\text{iso}}=r_{\text{iso}}^e+p_{\text{cyc}}'/p_c'$; $d\varepsilon_v^p=0$, p_c' remains constant). During the second part of the reloading (C-D), the yield surface is activated and plastic strains are produced to keep the yield limit on the stress point; r_{iso} increases according to Eq. (16) and produces a shift of the yield limit. When p_c' is reached, the conventional hardening of the yield limit occurs again (D-E) ($r_{\text{iso}}=1$; $d\varepsilon_v^p>0$, p_c' increases).

Thus, the preconsolidation pressure can be seen as the pressure for which the isotropic mechanism is totally active. Indeed, when $p'=p_c'$ in Eq. (15), the degree of mobilization of the isotropic mechanism r_{iso} is equal to one.

Appendix II. Consistency Equations

Eq. (32) expresses Prager's consistency condition for multiple dissipation processes

$$\mathbf{dF}=\frac{\partial \mathbf{F}}{\partial \boldsymbol{\sigma}'}:d\boldsymbol{\sigma}'+\frac{\partial \mathbf{F}}{\partial T}\,.\,dT+\frac{\partial \mathbf{F}}{\partial \boldsymbol{\pi}}\cdot\frac{\partial \boldsymbol{\pi}}{\partial \boldsymbol{\lambda}^{\mathbf{p}}}\cdot\boldsymbol{\lambda}^{\mathbf{p}}$$
$$=\mathbf{s}:d\boldsymbol{\sigma}'+\mathbf{t}\,.\,dT-\mathbf{H}\,.\,\boldsymbol{\lambda}^{\mathbf{p}}\le 0;\quad \boldsymbol{\lambda}^{\mathbf{p}}\ge 0;\quad \mathbf{dF}\,.\,\boldsymbol{\lambda}^{\mathbf{p}}\ge 0 \qquad (42)$$

The ACMEG-T model counts two dissipative processes coupled through their hardening parameters (r_{iso} and ε_v^p for the isotropic plastic mechanism and r_{dev} and ε_v^p for the deviatoric plastic mechanism). Therefore, the matrix of hardening moduli, $\mathbf{H}$, has the following expression:

$$\mathbf{H}=\begin{bmatrix} H_{ii} & H_{id} \\ H_{di} & H_{dd} \end{bmatrix} \quad \text{with}$$

$$\begin{cases} H_{ii}=-\dfrac{\partial f_{\text{iso}}}{\partial r_{\text{iso}}}\dfrac{\partial r_{\text{iso}}}{\partial \lambda_{\text{iso}}^p}-\dfrac{\partial f_{T\ \text{iso}}}{\partial \varepsilon_v^p}\dfrac{\partial \varepsilon_v^p}{\partial \lambda_{\text{iso}}^p}=p_c'\dfrac{(1-r_{\text{iso}})^2}{c}+p_c'\beta r_{\text{iso}} \\ H_{id}=-\dfrac{\partial f_{\text{iso}}}{\partial r_{\text{dev}}}\dfrac{\partial r_{\text{dev}}}{\partial \lambda_{\text{dev}}^p}-\dfrac{\partial f_{\text{iso}}}{\partial \varepsilon_v^p}\dfrac{\partial \varepsilon_v^p}{\partial \lambda_{\text{dev}}^p}=-\dfrac{\partial f_{\text{iso}}}{\partial \varepsilon_v^p}\dfrac{\partial \varepsilon_v^p}{\partial \lambda_{\text{dev}}^p}=p_c'\beta r_{\text{iso}}\dfrac{1}{Mp'}\left(M-\dfrac{q}{p'}\right)\alpha \\ H_{di}=-\dfrac{\partial f_{\text{dev}}}{\partial r_{\text{iso}}}\dfrac{\partial r_{\text{iso}}}{\partial \lambda_{\text{iso}}^p}-\dfrac{\partial f_{\text{dev}}}{\partial \varepsilon_v^p}\dfrac{\partial \varepsilon_v^p}{\partial \lambda_{\text{iso}}^p}=-\dfrac{\partial f_{\text{dev}}}{\partial \varepsilon_v^p}\dfrac{\partial \varepsilon_v^p}{\partial \lambda_{\text{iso}}}=Mp'b\beta r_{\text{dev}} \\ H_{dd}=-\dfrac{\partial f_{\text{dev}}}{\partial r_{\text{dev}}}\dfrac{\partial r_{\text{dev}}}{\partial \lambda_{\text{dev}}^p}-\dfrac{\partial f_{\text{dev}}}{\partial \varepsilon_v^p}\dfrac{\partial \varepsilon_v^p}{\partial \lambda_{\text{dev}}^p}=-\left(1-b\ln\dfrac{p'd}{p_c'}\right)\dfrac{(1-r_{\text{dev}})^2}{a}-b\beta\left(M-\dfrac{q}{p'}\right)\alpha r_{\text{dev}} \end{cases} \qquad (43)$$

The elastoplastic framework [Eq. (3)] enables the stress increment response with respect to prescribed strain increment to be expressed as

$$d\boldsymbol{\sigma}'=\mathbf{E}:(d\boldsymbol{\varepsilon}-d\boldsymbol{\varepsilon}_{\mathbf{T}}^{\mathbf{e}}-\mathbf{m}\,.\,\boldsymbol{\lambda}^{\mathbf{p}})=\mathbf{E}:(d\boldsymbol{\varepsilon}-\boldsymbol{\beta}_{\mathbf{T}}dT-\mathbf{m}\,.\,\boldsymbol{\lambda}^{\mathbf{p}}) \qquad (44)$$

where $\mathbf{E}$=current elastic stiffness tensor of the material, $\mathbf{m}$ defines the collection of flow directions; $\mathbf{m}=\partial\mathbf{G}/\partial\boldsymbol{\sigma}'$ with $\mathbf{G}$ being the potential vector function.

So, the consistency equation can be rewritten as follows:

$$\mathbf{dF} = \mathbf{s}:\mathbf{E}:d\boldsymbol{\varepsilon} - \overline{\mathbf{H}} \,.\, \boldsymbol{\lambda}^{\mathbf{p}} - \mathbf{H}_{\mathbf{T}} \,.\, dT \leq 0; \quad \boldsymbol{\lambda}^{\mathbf{p}} \geq 0; \quad \mathbf{dF} \,.\, \boldsymbol{\lambda}^{\mathbf{p}} \geq 0 \tag{45}$$

where

$$\overline{\mathbf{H}} = \mathbf{H} + \mathbf{s}:\mathbf{E}:\mathbf{m} \quad \text{and} \quad \mathbf{H}_{\mathbf{T}} = \mathbf{s}:\mathbf{E}:\boldsymbol{\beta}_{\mathbf{T}} - \mathbf{t} \tag{46}$$

$$\text{with} \quad \mathbf{E} = \begin{bmatrix} K+\frac{4}{3}G & K-\frac{2}{3}G & K-\frac{2}{3}G & 0 & 0 & 0 \\ & K+\frac{4}{3}G & K-\frac{2}{3}G & 0 & 0 & 0 \\ & & K+\frac{4}{3}G & 0 & 0 & 0 \\ & \text{sym} & & G & 0 & 0 \\ & & & & G & 0 \\ & & & & & G \end{bmatrix} \tag{47}$$

$$d\boldsymbol{\sigma}' = \left(d\sigma'_{11} \quad d\sigma'_{22} \quad d\sigma'_{33} \quad d\sigma'_{12} \quad d\sigma'_{13} \quad d\sigma'_{23}\right)^T \tag{48}$$

$$d\boldsymbol{\varepsilon} = \left(d\varepsilon_{11} \quad d\varepsilon_{22} \quad d\varepsilon_{33} \quad d\gamma_{12} \quad d\gamma_{13} \quad d\gamma_{23}\right)^T \tag{49}$$

$$\mathbf{dF} = \begin{pmatrix} df_{\text{iso}} \\ df_{\text{dev}} \end{pmatrix} \tag{50}$$

$$\boldsymbol{\lambda}^{\mathbf{p}} = \begin{pmatrix} \lambda^{p}_{\text{iso}} \\ \lambda^{p}_{\text{dev}} \end{pmatrix} \tag{51}$$

$$\mathbf{s} = \begin{pmatrix} \frac{\partial f_{\text{iso}}}{\partial \sigma'_{11}} & \frac{\partial f_{\text{iso}}}{\partial \sigma'_{22}} & \frac{\partial f_{\text{iso}}}{\partial \sigma'_{33}} & \frac{\partial f_{\text{iso}}}{\partial \sigma'_{12}} & \frac{\partial f_{\text{iso}}}{\partial \sigma'_{13}} & \frac{\partial f_{\text{iso}}}{\partial \sigma'_{23}} \\ \frac{\partial f_{\text{dev}}}{\partial \sigma'_{11}} & \frac{\partial f_{\text{dev}}}{\partial \sigma'_{22}} & \frac{\partial f_{\text{dev}}}{\partial \sigma'_{33}} & \frac{\partial f_{\text{dev}}}{\partial \sigma'_{12}} & \frac{\partial f_{\text{dev}}}{\partial \sigma'_{13}} & \frac{\partial f_{\text{dev}}}{\partial \sigma'_{23}} \end{pmatrix} \tag{52}$$

$$\mathbf{m} = \begin{pmatrix} \frac{\partial g_{\text{iso}}}{\partial \sigma'_{11}} & \frac{\partial g_{\text{iso}}}{\partial \sigma'_{22}} & \frac{\partial g_{\text{iso}}}{\partial \sigma'_{33}} & \frac{\partial g_{\text{iso}}}{\partial \sigma'_{12}} & \frac{\partial g_{\text{iso}}}{\partial \sigma'_{13}} & \frac{\partial g_{\text{iso}}}{\partial \sigma'_{23}} \\ \frac{\partial g_{\text{dev}}}{\partial \sigma'_{11}} & \frac{\partial g_{\text{dev}}}{\partial \sigma'_{22}} & \frac{\partial g_{\text{dev}}}{\partial \sigma'_{33}} & \frac{\partial g_{\text{dev}}}{\partial \sigma'_{12}} & \frac{\partial g_{\text{dev}}}{\partial \sigma'_{13}} & \frac{\partial g_{\text{dev}}}{\partial \sigma'_{23}} \end{pmatrix}^T \tag{53}$$

$$\boldsymbol{\beta}_{\mathbf{T}} = \begin{pmatrix} \frac{\beta'_s}{3} & \frac{\beta'_s}{3} & \frac{\beta'_s}{3} & 0 & 0 & 0 \end{pmatrix}^T \tag{54}$$

$$\mathbf{t} = \begin{pmatrix} \frac{\partial f_{\text{iso}}}{\partial T} \\ \frac{\partial f_{\text{dev}}}{\partial T} \end{pmatrix} = \begin{pmatrix} p'_{cT0}\frac{\gamma_T}{T \ln 10} r_{\text{iso}} \\ \frac{M r_{\text{dev}} p' b \gamma_T}{\left[1 - \gamma_T \log\left(\frac{T}{T_0}\right)\right] T \ln 10} + p'\left[1 - b \ln\left(\frac{p'd}{p'_c}\right)\right] g r_{\text{dev}} \end{pmatrix} \tag{55}$$

References

Abuel-Naga, H. M., Bergado, D. T., and Bouazza, A. (2007). "Thermally induced volume change and excess pore water pressure of soft Bangkok clay." *Eng. Geol. (Amsterdam)*, 89(1–2), 144–154.

Abuel-Naga, H. M., Bergado, D. T., Ramana, G. V., Grino, L., Rujivipat, P., and Thet, Y. (2006). "Experimental evaluation of engineering behavior of soft Bangkok clay under elevated temperature." *J. Geotech. Geoenviron. Eng.*, 132(7), 902–910.

Brandl, H. (2006). "Energy foundations and other thermo-active ground structures." *Geotechnique*, 56(2), 81–122.

Burger, A., Recordon, E., Bovet, D., Cotton, L., and Saugy, B. (1985). "Thermique des nappes souterraines." *Presses polytechniques universitaires romandes*, PPUR, Lausanne, Switzerland.

Campanella, R., and Mitchell, J. (1968). "Influence of temperature on soil behavior." *J. Soil Mech. and Found. Div.*, 94, 709–734.

Cekerevac, C., and Laloui, L. (2004). "Experimental study of the thermal effects on the mechanical behaviour of a clay." *Int. J. Numer. Analyt. Meth. Geomech.*, 28, 209–228.

Cui, Y. J., Sultan, N., and Delage, P. (2000). "A thermomechanical model for saturated clays." *Can. Geotech. J.*, 37, 607–620.

Dafalias, Y., and Herrmann, L. (1980). "A bounding surface soil plasticity model." *Proc., Int. Symp. Soils under Cyclic Transient Loading*, G. N. Pande and O. C. Zienkiewicx, eds., Balkema, Rotterdam, 335–345.

Eriksson, L. G. (1989). "Temperature effects on consolidation properties of sulphide clays." *Proc., 12th Int. Conf. on Soil Mechanics and Foundation Engineering*, Rio de Janeiro, Balkema, Rotterdam, Brookfield, 2087–2090.

Hueckel, T., and Borsetto, M. (1990). "Thermo-plasticity of saturated soils and shales: Constitutive equations." *J. Geotech. Engrg.*, 116(12), 1778–1796.

Hueckel, T., and Pellegrini, R. (1992). "Effective stress and water pressure in saturated clays during heating-cooling cycles." *Can. Geotech. J.*, 29, 1095–1102.

Hujeux, J. C. (1979). "Calcul numérique de problèmes de consolidation élastoplastique." Ph.D. thesis, Ecole Centrale de Paris, Paris.

Jamin, F. (2003). "Contribution à l'étude du transport de matière et de la rhéologie dans les sols non saturés à différentes températures." Ph.D. thesis, Université Montpellier II, Montpellier, France.

Koiter, W. T. (1960). "General theorems for elastic-plastic solids." *Progress in solid mechanics*, I. N. Sneddon and R. Hill, eds., North-Holland, Amsterdam, The Netherlands, 167–221.

Laloui, L. (1993). "Modélisation du comportement thermo-hydro-mécanique des milieux poreux anélastique." Ph.D. thesis, Ecole Centrale de Paris, Paris.

Laloui, L., and Cekerevac, C. (2003). "Thermo-plasticity of clays: An isotropic yield mechanism." *Comput. Geotech.*, 30(8), 649–660.

Laloui, L., and Cekerevac, C. (2008a). "Non-isothermal plasticity model for cyclic behaviour of soils." *Int. J. Numer. Analyt. Meth. Geomech.*, 32(5), 437–460.

Laloui, L., and Cekerevac, C. (2008b). "Numerical simulation of the non-isothermal mechanical behaviour of soils." *Comput. Geotech.*, 35(5), 729–745.

Laloui, L., and Modaressi, H. (2002). "Modelling of the thermo-hydro-plastic behaviour of clays." *Hydromechanical and thermohydromechanical behaviour of deep argillaceous rock*, Balkema, Rotterdam, The Netherlands, 161–170.

Laloui, L., Moreni, M., and Vulliet, L. (2003). "Behavior of a dual-purpose pile as foundation and heat exchanger." *Can. Geotech. J.*, 40(2), 388–402.

Laloui, L., Nuth, M., and Vulliet, L. (2006). "Experimental and numerical investigations of the behaviour of a heat exchanged pile." *Int. J. Numer. Analyt. Meth. Geomech.*, 30, 763–781.

Lewis, R. W., and Schrefler, B. A. (1987). *The finite element method in the deformation and consolidation of porous media*, Wiley, New York.

Mandel, W. (1965). "Généralisation de la théorie de Koiter." *Int. J. Solids Struct.*, 1, 273–295.

Mitchell, J. K. (1976). *Fundamentals of soil behavior*, Wiley, New York.
Mitchell, J. K., McMillan, J., Green, S., and Sisson, R. (1982). "Field testing of cable backfill systems." *Underground cable thermal backfill*, Pergamon, New York, 19–33.
Modaressi, H., and Laloui, L. (1997). "A thermo-viscoplastic constitutive model for clays." *Int. J. Numer. Analyt. Meth. Geomech.*, 21(5), 313–315.
Moritz, L. (1995). "Geotechnical properties of clay at elevated temperatures." *Swed. Geotech. Inst.*, 47.
Prager, W. (1958). "Non-isothermal plastic deformation." *Proc., Section of Sciences-B*, Vol. 61, Koninlijke Nederlandse Akademie van Wetenschapen, 176–182.
Rizzi, E., Maier, G., and Willam, K. (1996). "On failure indicators in multi-dissipative materials." *Int. J. Solids Struct.*, 33(20–22), 3187–3214.
Roscoe, K. H., and Burland, J. B. (1968). "On the generalized stress-strain behaviour of 'wet' clay." *Engineering plasticity*, J. Heyman and F. A. Leckie, eds., Cambridge University Press, Cambridge, England, 535–609.
Tidfors, M., and Sällfors, G. (1989). "Temperature effect on preconsolidation pressure." *Geotech. Test. J.*, 12, 93–97.
Vulliet, L., Laloui, L., and Schrefler, B. (2002). *Environmental geomechanics*, EPFL, Lausanne, Switzerland.